IJST, Transactions of Mechanical Engineering, Vol. 39, No. M2, pp 291-307
Printed in The Islamic Republic of Iran, 2015

FINITE ELEMENT MODELING AND EXPERIMENTAL STUDY OF RESIDUAL STRESSES IN REPAIR BUTT WELD OF ST-37 PLATES*

A. FADAEI** AND H. MOKHTARI

Dept. Mechanical Engineering, Engineering Faculty, Bu-Ali Sina University, Hamedan, I. R. Iran
Email: as.fadaei@gmail.com

Abstract– Welding is one of the most important assembling methods which are widely applied in different applications. In service conditions, some of the weld joints which meet defects must be repaired. The residual stresses impress the operation and efficiency of the repair weldment. In this study, the temperature and the residual stress fields were investigated by both the finite element simulation and the experimental measurement due to repair butt weld of the two thin St 37 plates. The welding process was simulated using the three-dimensional finite element and the Goldak double-ellipsoid heat source models. The temperature distribution and the residual stresses were computed both in the initial and repair welds. The element birth and death technique was used to simulate the filler metal deposition into the weld pool. The experimental measurements were performed to verify the numerical results in the both initial and repair welds. The residual stresses were measured using the hole drilling method. The experimental results revealed that the finite element simulations obtained in the present work were capable of predicting the residual stresses in the initial and repair welds. Also, the effect of the repair length variation on both magnitudes and distribution of the transverse and longitudinal residual stresses were shown.

Keywords– Repair butt weld, residual stress, finite element simulation, experimental study, hole drilling method

1. INTRODUCTION

Welding is one of the most prevalent methods in assembling the metal parts and is widely applied in the different fields of industry such as the oil and gas industries. High static strength, lightweight joint and short time of the treatment are some advantages of weld joints. In practice, making the non-defect weld joint is uneconomical. A weld joint does not behave exactly as designed and the defects and flaws would affect the performance of the weldment. In service conditions, some of the weld joints which meet defects must be repaired in order to regenerate the efficiency of the component. In repair, the weld containing the defects is excavated through grinding and then is welded again. Like the initial welding, the repair welding would have the critical effect on the lifetime of the component. This effect could be resulted from the residual stresses and the metallurgical transformations in the vicinity of the repaired zone. The residual stresses would destroy integration of the component. Furthermore, the high tensile residual stresses may also cause the stress corrosion cracking in the vicinity of the Heat Affected Zone (HAZ). Further, the residual stresses have a significant effect on the fatigue crack growth under loading [1].

The distribution of residual stresses in the repair welds can be different from that of the initial fabrication welds. The prediction of the residual stress distribution in the welding process is very complicated and there is no analytical solution to calculate it due to the highly nonlinear behavior. Hence, in the recent decades numerical methods, especially finite element method in welding process analysis and simulation have become interesting to researchers. Study on the thermal stresses of welding process began

*Received by the editors April 5, 2014; Accepted May 13, 2015.
**Corresponding author

in 1930 and the first solutions were presented in 1936. In these years, for the first time computer was used to simulate the thermal stresses. Rosenthal [2] was among the first researchers to develop the analytical solution of heat flow during welding based on heat conduction for predicting the shape of the weld pool for the two and three-dimensional modeling. Using the Fourier partial differential equation for the heat conduction, he introduced the moving coordinate system to develop the solutions for point and line modeling of the heat sources and successfully applied this to address a wide range of the welding problems.

In the previous century, researchers could compute the temperature and the residual stress fields numerically using thermo-elastic-plastic analysis. Because of the software and hardware weaknesses and high expenses, most of these simulations were restricted to the plane strain-stress and axisymmetric models and other simple ones like the 3D shell models. Friedman [3] presented the thermo-mechanical plane stress model for analyzing the welding process. In this research, distribution and distortion of the residual stress were achieved by analyzing the temperature fields of the welded plates. He presented the disk model to simulate arc of welding as the heat source for first time. The most critical input data required for the welding thermal analysis were the parameters to describe the heat input to the weld area from the arc. Goldak et al. [4] derived the mathematical model for welding heat sources based on the Gaussian distribution of power density. They proposed the doubled ellipsoidal distribution in order to capture size and shape of the heat source of the shallow and deeper penetrations. Michaleris and co-worker [5] developed the finite element model to predict the distortion in welding process and the following experimental measurement proved the computed numerical results. Tsai et al. [6] investigated effect of welding order on buckling and distortion of the thin plates. They also predicted the effect of the welding parameter variations on both magnitude and distribution of the residual stresses in the thick plates.

In the last two decades, predicting and measuring the residual stresses in repair welds have been attractive to researchers. Kim et al. [7] simulated the weld repairs on the thick plates by the finite element method using 2D and 3D models. They concluded that the shorter length of repair weld and the slower speed for welding created the higher transverse stress. Dong et al. [8] investigated the weld repairs in several cases in the pipes and the plates using the 3D shell model and the experimental measurement techniques. Their results showed that the shorter length of repair led to an increase in the transverse stresses. Also, they remarked that in the repair welds, the heat input quantity and the weld order were of more importance compared to the initial welds. Dong and co-workers [9] concluded that the residual stresses exhibited the three dimensional features in the repair weld that depended on the geometric specifications of both weld and weldment. Bouchard et al. [10] performed the experimental measurement to obtain the through thickness residual stresses distribution in the stainless steel pipes using the deep hole drilling and the neutron diffraction methods. Their results revealed that trend of the residual stresses in repair weld was opposite that of the initial weld. George and Smith [11] analyzed the through thickness residual stress distribution in the stainless steel cylinders containing the repair weld using the deep hole drilling method. They investigated whether the shapes of distribution were basically the same before and after repair weld. However, the repair increased the axial membrane residual stress at the mid-length of repair weld compared with the original girth weld. Brown et al. [12] who worked on the plate letterbox repair welds emphasized on the validation of the numerical modeling using the experimental residual stress measurement. They inferred that the 2D models can be used to indicate levels of the residual stress present in the transverse direction of the repair weld remote from the ends. However, 3D model simulations are required to determine the full detailed distribution and the end effects on the weld. Mirzaee-Sisan and co-workers [13] measured the residual stresses in the type 316H stainless steel steam header made using the deep hole drilling technique to characterize the through thickness residual stress distribution in the circumferentially repaired weld. The results highlighted the generation of high residual stresses due to repair the welding. Aloraier et al. [14] reviewed the half-bead and the cold repair technique practices and their consequences on the residual stresses within the nuclear, power, refinery and petrochemical industries. They reported the study on measuring the residual stresses using the neutron diffraction and it showed very little reduction in the residual stresses over the normally completed welds. Jiang et al. [15] used the finite element method to predict the residual stresses in the repair weld of the stainless steel clad plate. The results showed that the peak residual stress occurred in the heat affected zone of the base metal, because the yield strength of the base metal was larger than that of the clad metal. Also, with an increase in the repair width, the residual stresses were decreased. Jiang and co-workers [16] estimated the residual stress and the deformation in the repair weld of the stainless steel clad plate by the finite element method. The effects of the heat input and the welding layer number on residual stresses and deformation were studied. The results showed that large residual stresses were generated in the repair weld. With the heat input and the welding layer number increasing, the residual stresses were decreased. Jiang et al. [17] studied the effect of repair length on the residual stress, aiming to provide the reference for repairing the cracked clad plate. The results showed that large tensile residual stresses were generated in the repair weld and the heat affected zone, and then decreased gradually away from the weld and the heat affected zone. Roshani et al. [18] studied the temperature distribution of an AISI 304 stainless steel during gas tungsten arc welding modeled by using the Goldak's three-dimensional moving heat source. By simulating the temperature distribution and shape of the weld pool, effect of welding parameters such as current and welding speed on the sensitization, weld width and weld depth are evaluated. Fadaei and Jokar [19] investigated the variations of yield stress, hardness and microstructures in the A 36 repair butt specimens by the experimental study. The mean of yield stresses in the specimens were reduced after the repairing through half- thickness of the butt welds. Moreover, the mean of yield stresses in the specimens after repairing would be decreased if the welding voltage and current increased. Reduction of the hardness in heat affected zone and variation of the phases and grain size after repairing were other outcomes from testing on the specimens.

In this study, distribution of residual stress in the one-pass repair weld in the St-37 steel plates was investigated. St 37 was selected as the material for the welding plates. This material has numerous applications in manufacturing the various structures and the parts such as bridges, steel structures, auto parts and industrial machines components. The 3D finite element model was investigated and the residual stresses in both initial fabrication and the repair welds were obtained. The numerical results were verified using the experimental measurement. The residual stresses were measured using the hole drilling method.

2. THE WELD JOINT GEOMETRY AND WELDING PARAMETERS

Two St-37 plates with dimension of 250 mm in length, 100 mm in width and 3 mm in thickness were butt welded by the Metal Insert Gas (MIG) welding method using ER70S-6 electrodes. The chemical combinations of the base metal and the electrode are shown in Table 1.Figure 1 shows the schematic presentation of welding samples in this study and the pictures of the completed joint in the initial and repair welds. The repair zone was selected the central one-third length of the plate. The repair was accomplished through the whole plate thickness.

Table 1. Chemical composition of electrode and base metal

Grade	Fe	C	Mn	Si	P	S	Cr	Mo	Ni	Co	Cu
St-37	Base	0.130	0.570	0.200	0.010	0.012	0.002	0.010	0.030	0.001	-
ER70S-6	Base	0.070-0.150	1.400-1.850	0.800-1.150	0.025	0.350	-	-	-	-	0.500

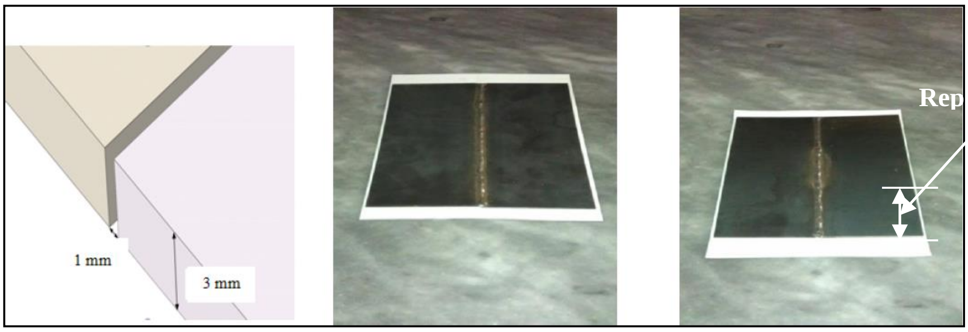

(a) (b) (c)

Fig. 1. (a) Joint geometry, (b) The specimen after initial weld, (c) The specimen after repair weld

3. THERMO-MECHANICAL ANALYSIS

Thermal and mechanical fields impress welding process. Since heat that arises from plastic strain is insignificant, the thermal and mechanical analysis could be accomplished independently. So, modeling of the arc welding process may be divided into two steps: heat transfer and mechanical analysis. In all performed modeling in this paper, the effect of phase transformation was ignored [20]. In both thermal and mechanical analysis temperature dependent the thermo-physical and mechanical properties of the base metal were used in the computations. The material properties of St 37-2 as the function of temperature, including thermal conductivity, specific heat, yield stress, elastic modulus, Poisson's ratio and thermal expansion coefficient were shown in Fig. 2 [21]. The detailed welding conditions is shown in Table 2. The welding conditions were the same in both the initial and repair welds.

Table 2. Welding conditions

Parameter	Current (A)	Voltage (V)	Welding speed (mm/s)	Wire (electrode) diameter (mm)
Value	120	22	6	0.8

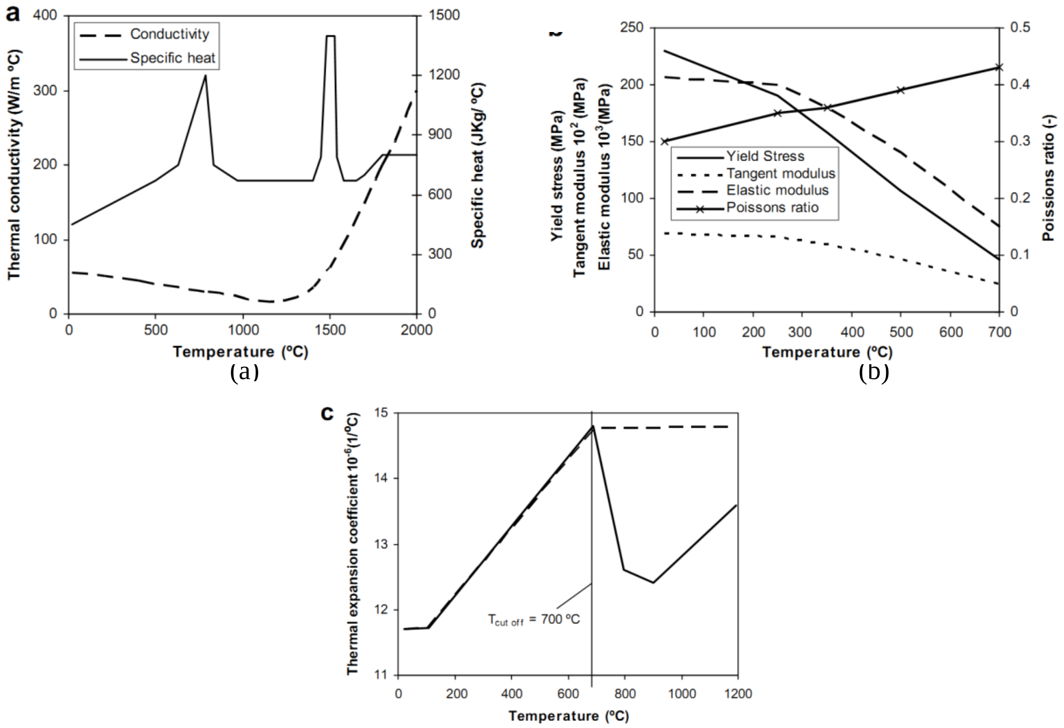

(a) (b)

(c)

Fig. 2. The material properties of St 37-2, (a) Thermal conductivity, (b) Mechanical properties, (c) Thermal expansion coefficient [21]

a) Thermal analysis

The thermal transfer of welding process is a time-dependent problem. The heat conduction was assumed to be governed by Fourier law:

$$\rho c_p \frac{\partial T}{\partial t} = \frac{\partial}{\partial x}\left(k_x \frac{\partial T}{\partial x}\right) + \frac{\partial}{\partial y}\left(k_y \frac{\partial T}{\partial y}\right) + \frac{\partial}{\partial z}\left(k_z \frac{\partial T}{\partial z}\right) + \dot{q_v} \tag{1}$$

In this equation ρ denotes the density (kg/m^3), c_p is the pressure-constant specific heat (J/kg.K), T is temperature (K), t is time (s), k is the temperature-dependent thermal conductivity (J/m.s.K), and $\dot{q_v}$ is the rate of internal heat generation (W/m^3.s). Two kinds of the boundary condition including convection and radiation were considered in the thermal analysis. The surface convection according to the Newton's law is given by:

$$q_{con} = h_{con}(T_s - T_\infty) \tag{2}$$

Where h_{con} is the film coefficient of convection (J/K.m^2), T_s is the surface temperature of plate (K) and T_∞ is the ambience temperature (K). It was assumed that the ambience temperature is 298 K (25 °C). Another surface effect is the heat loss due to radiation and according to the Stefan-Boltzmann law it is given by:

$$q_{rad} = \varepsilon\sigma(T_s^4 - T_\infty^4) \tag{3}$$

Where ε is the surface emissivity constant and σ is the Stefan-Boltzmann coefficient (J/K^4.m^2). Deng [22] represented the total temperature-dependent film coefficient by combining both convection and radiation effects as:

$$h = o.68 \quad \left(\frac{W}{m^2}\right) \qquad if \quad 0 < T < 500\ ℃ \tag{4a}$$

$$h = 0.231T - 82.1 \quad \left(\frac{W}{m^2}\right) \qquad if \quad T > 500\ ℃ \tag{4b}$$

b) Mechanical analysis

In numerical analyses of welding using the thermal, elastic and plastic models are always necessary in order to predict the residual stresses. Since phase transformations take place at a relatively high temperature for the mild steels such as St 37, the volume change and hence the phase transformations can be ignored. Thus, with these assumptions the total strain is composed of an elastic, plastic and thermal part as:

$$\varepsilon_{total} = \varepsilon_e + \varepsilon_p + \varepsilon_t \tag{5}$$

Considering the Eq. (5), the constitutive equation may be expressed as follows:

$$\sigma = D\varepsilon_e = D(\varepsilon_{total} - \varepsilon_p - \varepsilon_t) \tag{6}$$

where D is the material stiffness matrix. The elastic-plastic behavior with the linear kinematic hardening was used as the material model. For typical mild steels, St 37, the yield stress considerably reduced with increasing temperature and naturally vanished at the melting temperature.

4. FINITE ELEMENT MODEL

In this research, for finite element modeling – ABAQUS 6.10 software was applied to fulfill the thermal and mechanical analyses. Because of the symmetry of the welded plates only one of them was modeled. Figure 3 illustrates the mesh configuration of the weld plate in the thermal and mechanical analyses. Due to the presence of the high temperature and the stress gradient near the weld line, a relatively finer mesh was provided and the element size was increased progressively with distance from the weld line. The element birth and death technique was used to simulate the weld passes and the filler metal deposition into the weld pool. In the finite element analysis 8300 eight-node hexahedral elements are used to make the 3D meshing of the geometry for the thermal and mechanical analyses.

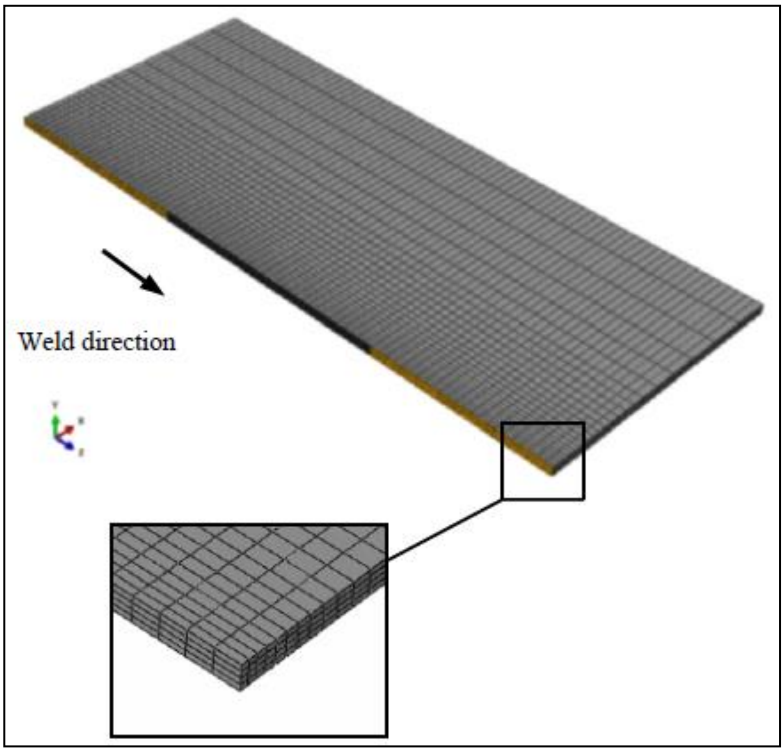

Fig. 3. Finite element model

The parameters that are used to model the thermal source resulting from electrical arc are the most important parameters to analyze the welding process. These parameters are the heat input distribution, the size of the Fusion Zone (FZ) and Heat Affected Zone (HAZ), rate of the cooling and thermal gradients. The welding heat input or the electrical power of welding arc was calculated using the following equation:

$$Q = \eta V I \tag{7}$$

where η is the arc the efficiency, *V* is the voltage and I is the current of the welding process.

The Goldak double-ellipsoid heat source model [4] was adopted to calculate the volumetric heat flux distribution as the input heat into the welding pool. The heat source distribution as shown in Fig. 4 combines two different ellipses, i.e. one in the front quadrant of the heat source and the other in the rear quadrant of it. The power densities of the double-ellipsoid heat source, $q_f(x, y, z)$ and $q_r(x, y, z)$, describing the heat flux distribution inside the front and rear quadrant of the heat source, can be expressed as [23]:

$$q_f = \frac{6\sqrt{3}Qf_f}{abc_f\pi\sqrt{\pi}} e^{-3\left(\frac{x^2}{a^2}\right)} e^{-3\left(\frac{y^2}{b^2}\right)} e^{-3\left(\frac{z^2}{c_f^2}\right)} \tag{8}$$

$$q_r = \frac{6\sqrt{3}Qf_r}{abc_r\pi\sqrt{\pi}} e^{-3\left(\frac{x^2}{a^2}\right)} e^{-3\left(\frac{y^2}{b^2}\right)} e^{-3\left(\frac{z^2}{c_r^2}\right)} \tag{9}$$

In the above equations, *a* is the weld width along the tangent direction *x*; *b* is the weld penetration depth along the arc direction *y*; c_f and c_r are the forward and rear weld pool lengths in the weld path direction *z*; and f_f and f_r are some dimensionless factors.

To calculate *a* and *b*, the cross section of the weld was prepared, as shown in Fig. 5. Two parameters, c_f and c_r were determined using the following relationships [23]:

$$c_f \in (0.5a, a) \quad \& \quad c_r \in (2a, 4a) \tag{10}$$

Two dimensionless factors f_f and f_r were obtained from the following equations [23]:

$$f_f = \frac{2c_f}{c_f + c_r} \quad \& \quad f_r = \frac{2c_r}{c_f + c_r} \tag{11}$$

The parameters of the heat flux distribution were calculated using the above discussion and are shown in Table 3.

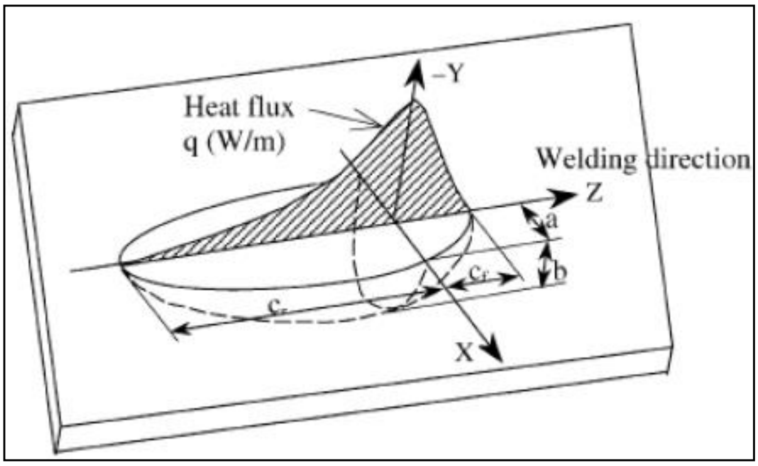

Fig. 4. The Goldak double-ellipsoid heat source model [4]

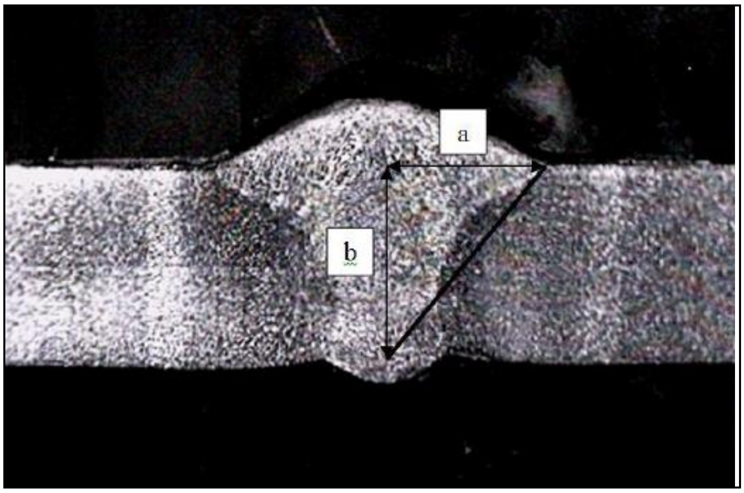

Fig. 5. The cross section of the weld

Table 3. The parameters of the heat flux distribution

Parameter	a (mm)	b (mm)	c_f (mm)	c_r (mm)	f_f	f_r
value	2.5	3	2.5	7.5	0.5	1.5

The mechanical analysis was conducted based on the thermal analysis results. The nodal temperatures from the associated transient heat transfer analysis were the only applied loads to the stress analysis. Since the inertia has an insignificant effect on the mechanical performance of the plate, the static stress analysis was adopted in this study. Due to the heating and cooling cycle in the initial and repair welding, the kinematic hardening was used in the finite elements simulations.

As shown in Fig. 5, the weld plate was restrained against motion by the fixture. In mechanical analysis, boundary conditions are used to prevent the rigid body motion. Because of the symmetry of the finite element model, the symmetric plane is fixed in x-direction. The one edge was constrained in both x-and z-directions; and the other edge was constrained only in y-direction. Also, parts of the plate that were in contact with the fixture were constrained in y-direction. It should be noted that weld repair was considered under the same constraint condition.

Before performing the repair welding, the stress relief operations were applied to the experimental specimens. So, in the finite element simulation of the weld repair it was assumed that the models were free of the residual stresses. As a result, the repair welding simulation was the same as the initial welding. Of course, the finite element simulation of the repair welding was performed for the part of the initial weld line. The element birth and death technique was used to remove the repair zone and to create the repair weld. In this technique, first, to eliminate the repair zone the elements were removed and then to create the repair weld they were reproduced to simulate the weld passes and the filler metal deposition into the weld pool.

5. EXPERIMENTAL STUDY

In order to verify the numerical results, the experimental measurement of residual stresses using the hole-drilling method was performed at the corresponding positions in the initial and repair welds which are displayed schematically in Fig. 6. The measurement was performed in the middle-section of the plate with distance equal to 2.7 mm from the weld line. The specimen with the bonded rosette strain gage is shown in Fig. 7. The most widely used modern technique for measuring residual stress is the hole- drilling strain-gage method of stress relaxation. The introduction of a hole (even of very small diameter) into a residually stressed body relaxes the stresses at that location. This occurs because a perpendicular axis to every hole surface is necessarily a principal axis on which the shear and normal stresses are zero. The elimination of these stresses on the hole surface changes the stress in the immediately surrounding region, causing the local strains on the surface of the test object to change correspondingly. This principle is the foundation for the hole-drilling method of residual stress measurement. The procedure is relatively simple, and has been standardized in ASTM Standard Test Method E 837.

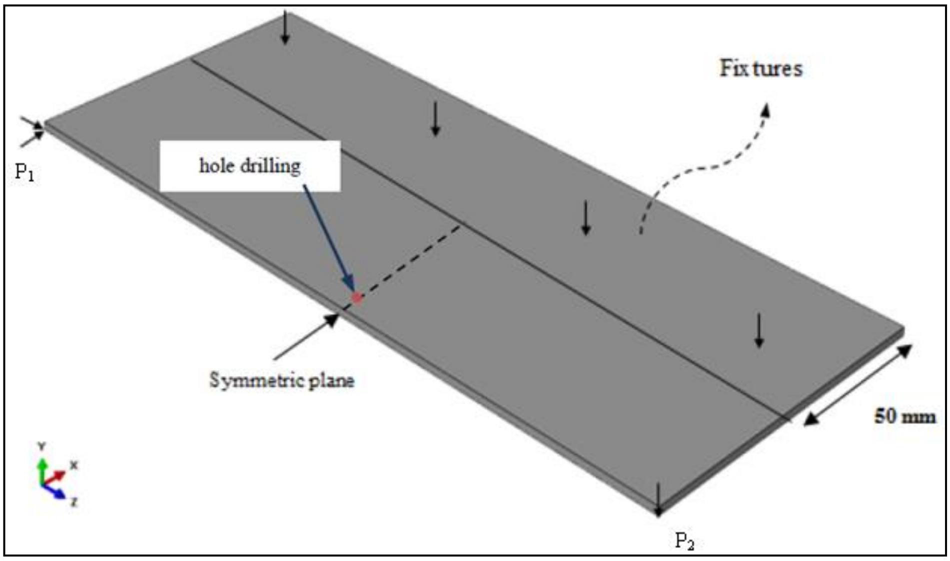

Fig. 6. Schematic presentation of mechanical boundary conditions

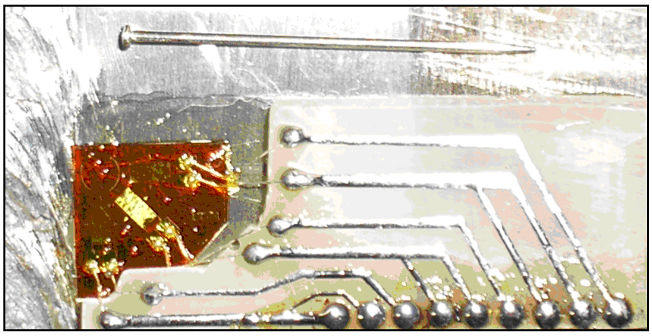

Fig. 7. Presentation of the bonded strain gage on the specimen

6. RESULTS OF FE ANALYSIS

Figure 8 shows the temperature distribution on the welded plate after 20.5 seconds from welding start when the heat source (electrical arc) was at a distance of 125 mm from the edge of plate. It was evident from Fig. 8 that the temperature around the torch reached 1827°C. The input heat to the weldment gradually transferred to the rest of the base plate in all directions due to conduction. The thermal distribution which was attained via the Goldak thermal model indicated that the highest temperature was attained at the torch location which was also consistent with the experimental observations. Also, the cooling effects can be visualized by the decreasing temperature of the weld start position where the temperature drops around 325°C.

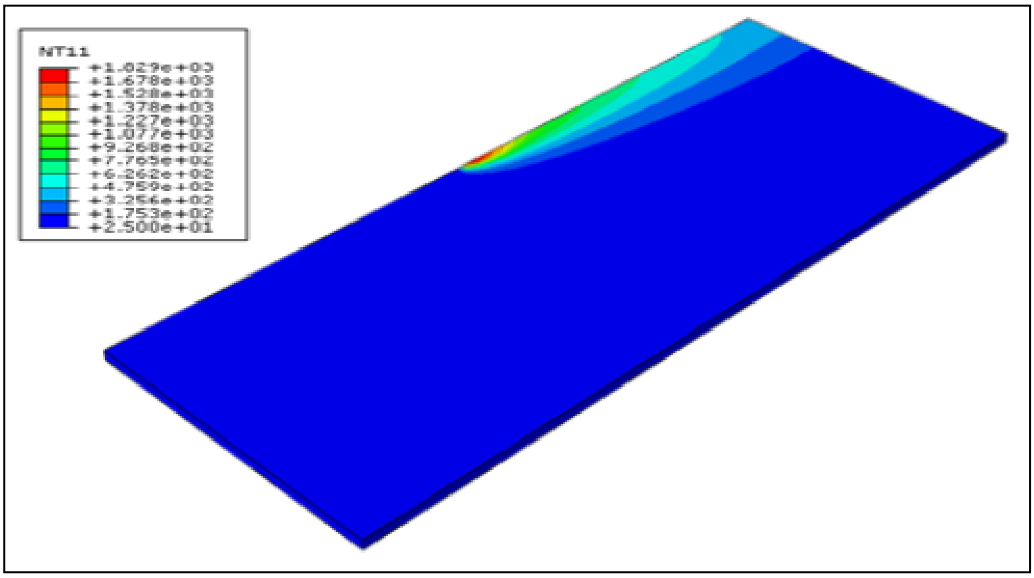

Fig. 8. Temperature distribution of welded plate after 20.5 seconds from welding start

Figure 9 shows the temperature histories of the three points at FZ, HAZ and out of HAZ, respectively after 8 seconds from the beginning time of welding. It is important to note that the reduction of temperature with the distance has a nonlinear trend. The reason is associated with the local heating of the welding arc and the nonlinear variation of the material's thermal properties with temperature. After a certain time, three curves coincide which is indicative of the same temperature in these areas.

Figure 10 shows the temperature distribution on the top surface of the welded plate along the transverse direction at different time. It shows that the temperature in the FZ was substantially higher when the welding torch just passed the plane but it decreased quickly with time. The temperatures in HAZ were increased gradually with time when the heat in the FZ was transferred through conduction.

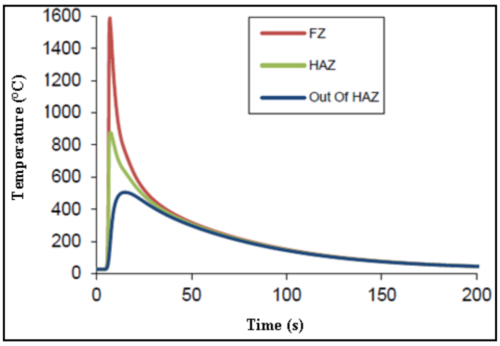

Fig. 9. Temperature histories in three zones

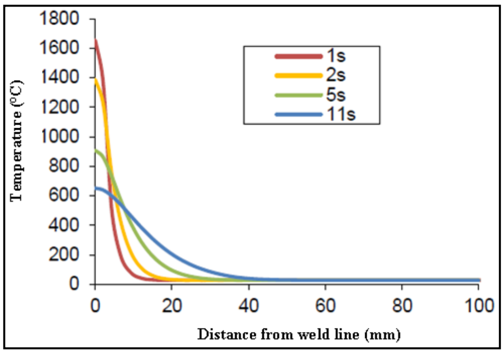

Fig. 10. Temperature distribution on the top surface of the welded plate along transverse direction

Figure 11 shows the distribution of the transverse and longitudinal residual stresses on the top surface using the fixture for clamping of the plates in the initial welding. The distribution and magnitude of residual stresses in the plate were strongly dependent on the mechanical boundary conditions imposed by the welding fixtures. The maximum value of longitudinal residual stress was 256 MPa which was higher than the material tensile strength. The transverse residual stresses were much smaller than the longitudinal residual stresses at the two edges of the plate where the welding was started and ended in such a way that the transverse residual stresses had negative values (-244 MPa), indicating that the plate at the two ends experienced the compressive stresses.

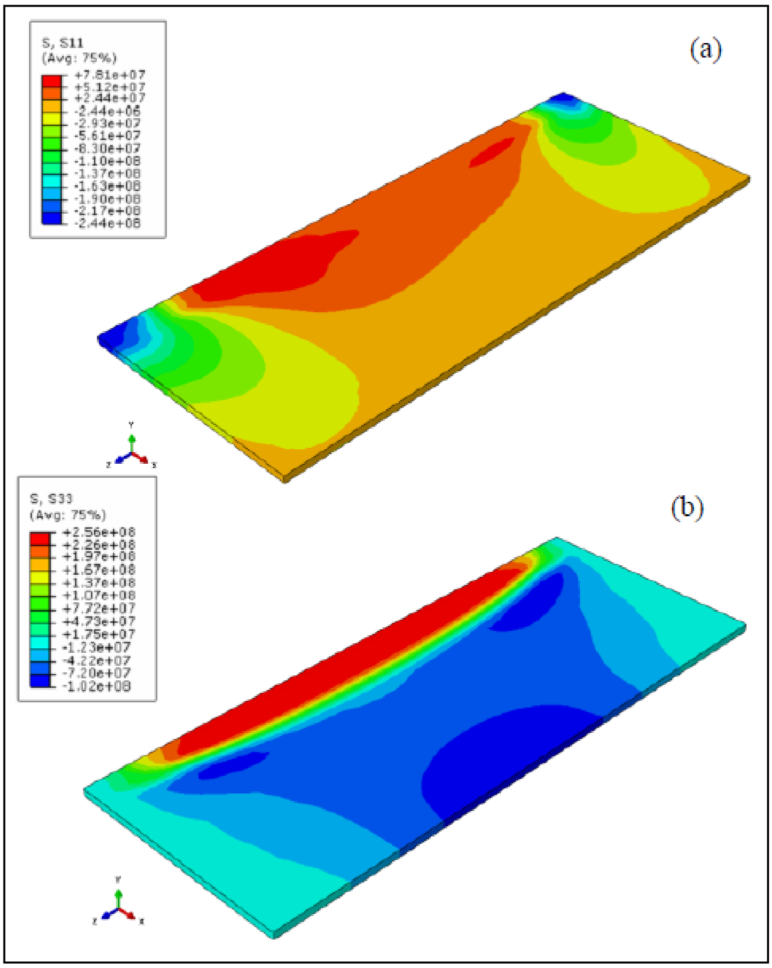

Fig. 11. Residual stresses in initial butt weld with the fixtures (a) Transverse residual stress and (b) Longitudinal residual stress

Figure 12 shows the distribution of transverse and longitudinal residual stresses on the top surface under the constraint condition in the repair weld. When the weld repair with short length was introduced at the mid-length of the initial butt-weld, this resulted in a strongly varying pattern for the transverse residual stress surrounding the repair. The magnitudes of transverse tensile residual stresses in the region of the repair were high and approached the tensile strength of the plate material. Moreover, the transverse residual stress field had a long sphere of influence in the transverse direction. Immediately beyond the repair start and stop positions, the two distinct compressive zones of the transverse stress were predicted. The two less marked tensile zones are also evident in the predicted distribution of the longitudinal stresses beyond the repair start and the stop position, but the overall distribution was broadly similar to that of the initial butt weld.

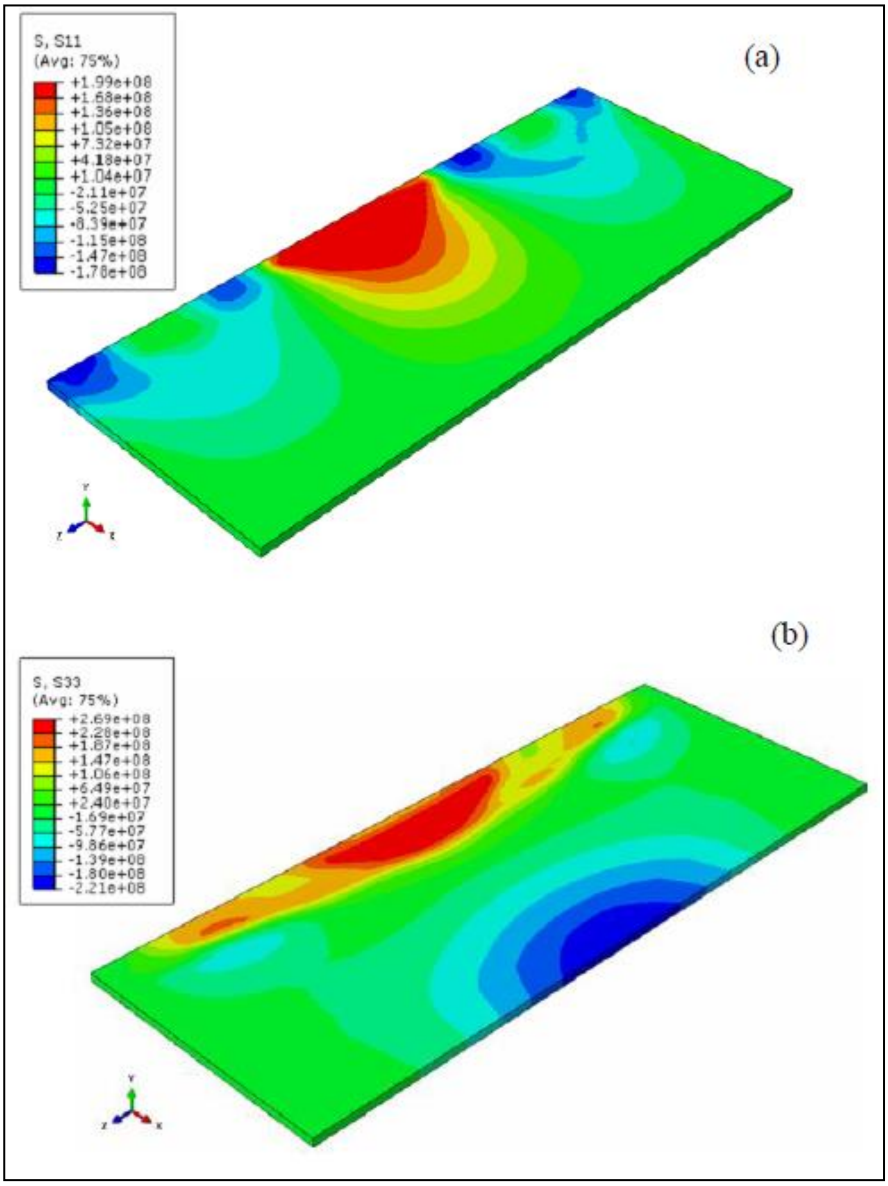

Fig. 12. Residual stresses in repair butt weld with the fixtures (a) Transverse residual stress and (b) Longitudinal residual stress

Figures 13 and 14 show the transverse and longitudinal stresses in the middle-section of the plate in the repair and the initial welds using the fixtures respectively. The effects of repair on the magnitude of longitudinal residual stress are not significant and trend of the longitudinal stress was almost the same in both the initial and repair welds. On the contrary, introduction of the repair significantly increased the transverse residual stresses. The maximum value of transverse stress in the weld repair was much more than its maximum value in the initial weld, although the overall trend of both curves is similar to each other.

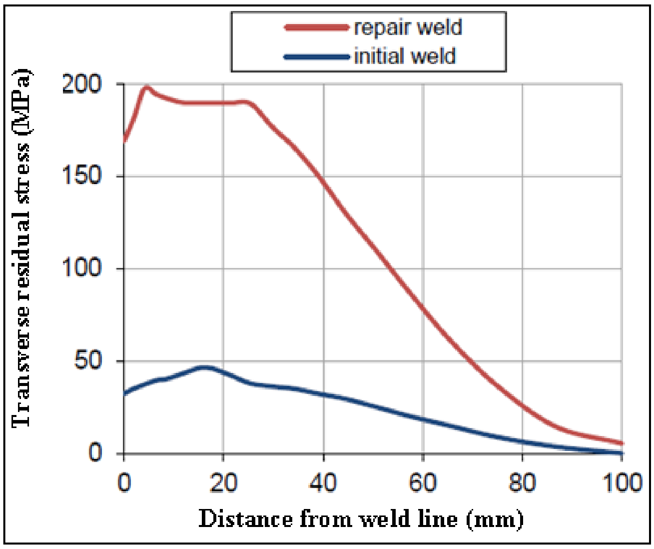

Fig. 13. Comparison of transverse residual stresses along x-axis in middle-section weld line

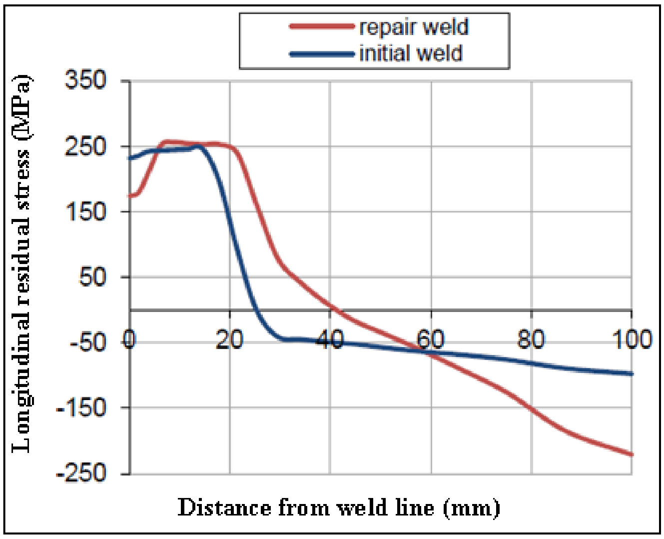

Fig. 14. Comparison of longitudinal residual stresses along x-axis in middle-section weld line

7. COMPARISON BETWEEN NUMERICAL AND EXPERIMENTAL RESULTS

Figures 15 and 16 show the transverse residual stress through thickness in the initial and repair welds, respectively. It can be seen that there is a typical agreement between the finite element predictions and the measured stresses for the transverse residual stress in the initial and repair welds. In a way that the finite element predictions mainly overestimated the transverse residual stress compared to the measured stresses at the middle-section of the plate.

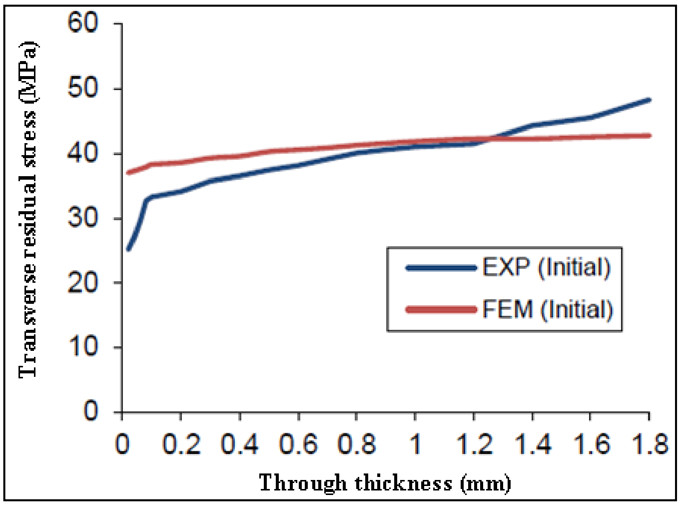

Fig. 15. Comparison of the transverse residual stress through thickness in initial weld

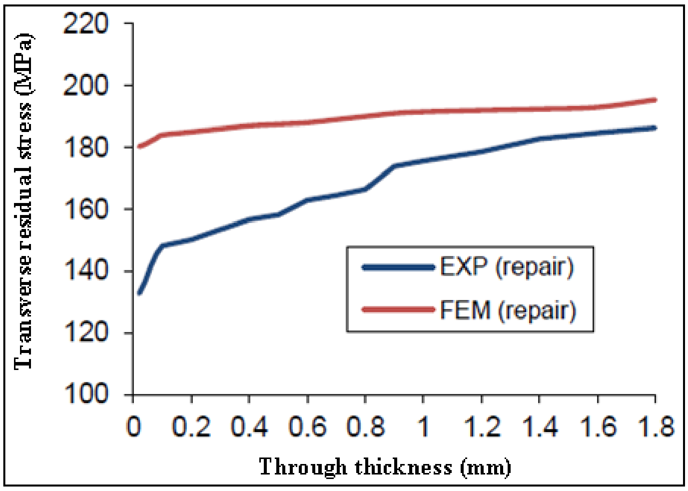

Fig. 16. Comparison of the transverse residual stress through thickness in repair weld

Comparison of the finite element predictions for the longitudinal residual stresses after the initial and repair welding are shown in Figs. 17 and 18, respectively. The longitudinal residual stress predictions to some extent agree with the measured values.

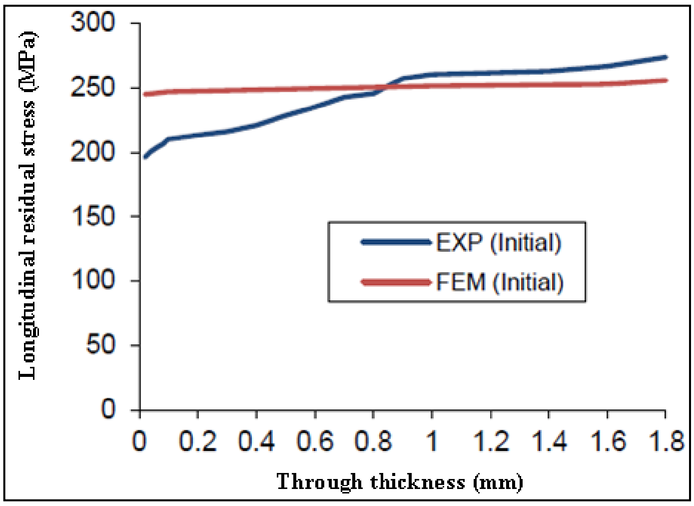

Fig. 17. The longitudinal residual stresses through thickness in middle-section for initial weld

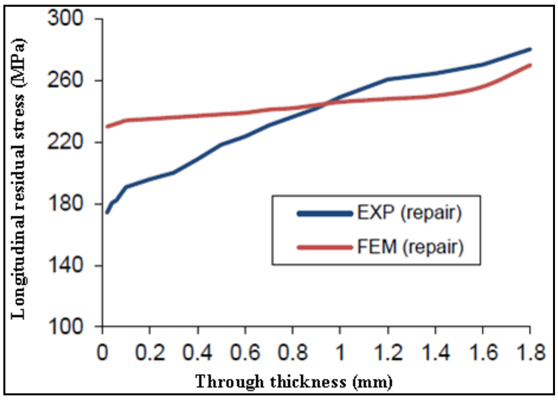

Fig. 18. The longitudinal residual stresses through thickness in middle-section for repair weld

8. EFFECT OF REPAIR LENGTH

In reality the length of a repair weld is crucial in determining the local residual stresses which it causes. This is obvious because, if the repair is sufficiently long for example, the whole length of initial weld line, then there is no distinction between a repair and a complete new weld. Hence, sufficiently long repairs will produce the same residual stress distribution as an unrepaired weld. In this study, keeping the remaining welding parameters constant, the other three models with 1/3, 1/2 and 1/2 repair length of initial weld line were built and calculated to investigate the influence of repair length on residual stress.

The transverse residual stress distribution in the middle-section of plate for three different repair lengths are shown in Fig. 19. As can be seen by increasing the repair length, the transverse residual stresses were decreased. In the short length of repair the values of the transverse residual stresses were high, but with increasing the repair length the transverse stresses within the central region of the repair length approached that of the initial weld.

The longitudinal residual stress distributions in three different repair lengths are shown in Fig. 20. It can be seen that variations in the repair length had no significant effect on the longitudinal stresses. This may be due to the heat source moving in the longitudinal direction during the welding and flowing of molten filler material to the weld line for the repair welding with different lengths. Also, the magnitude of longitudinal tensile residual stresses near the weld line approached the maximum possible value as the tensile strength of material for the different repair lengths. In Fig. 20, the magnitude and overall trend of the stresses in three cases were similar. All the distributions showed a peak for the tensile residual stress about 10 mm away from the weld centerline and gradually reduced to zero towards the outer rim of the plate.

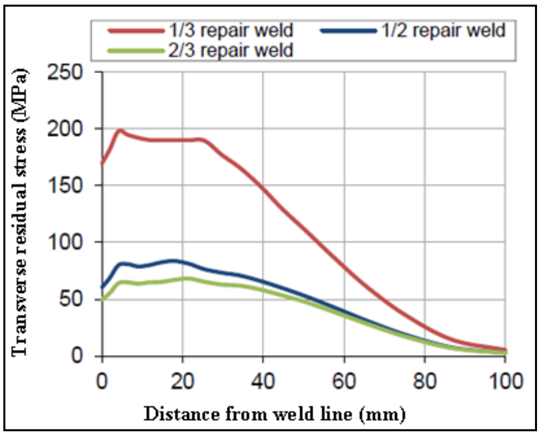

Fig. 19. The transverse residual stresses in middle-section of plate for three different repair lengths

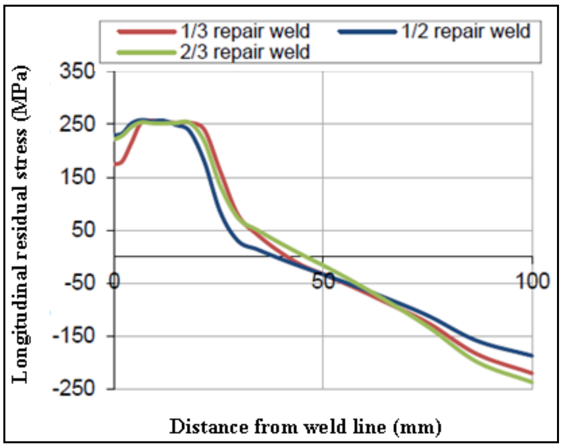

Fig. 20. The longitudinal residual stresses in middle-section of plate for three different repair lengths

9. CONCLUSION

In this work the repair weld of the thin St 37 steel plates was investigated. The thermo-elastic–plastic finite element simulation along with the Goldak double-ellipsoid heat flux model was used to predict the residual stresses in both the initial and repair welds. Also, the experimental measurement was performed for validating the numerical results. The following results are obtained from the studies conducted:

1. The input heat during the welding transferred quickly first in the thickness direction of the plate and then in the transverse and longitudinal directions to reach uniformed distribution. The temperature of the plate with increasing of distance from the weld line decreased as the nonlinear trend.
2. The temperature in the FZ was substantially higher when the welding torch just passed the plane but it decreased quickly with time. The temperatures in the HAZ were increased gradually with time when the heat in the FZ was transferred through conduction.
3. By applying fixtures during both initial and repair welds, the transverse residual stress gradually reduced toward the outer rim of the plate but the longitudinal residual stress changed from tensile to compressive with increasing distance from the weld line.
4. The magnitude of transverse tensile residual stresses in the region of the repair was high and approached that of the tensile strength of material. The tensile transverse residual stresses along the repair length sharply fell into compressive stress beyond the two ends of the repair weldment. The less marked tensile zones were also evident in the predicted distribution of the longitudinal residual stresses, but the overall distribution was broadly similar to that of the initial butt weld.
5. The shorter repair length caused the greater transverse residual stresses, but for long length repairs the transverse residual stresses within the central region of the repair length approached that of the initial weld.
6. The variation in the repair length had no significant effect on the longitudinal residual stresses. The magnitude and the overall trend of the stresses in the three study cases were similar.

REFERENCES

1. Shen, W. Y. & Clayton, P. (1996). Fatigue of fillet welded A515 Steel. *Engineering Fracture Mechanics*, Vol. 53, No. 6, pp. 1007-16.
2. Rosenthal, D. (1941). Mathematical theory of heat distribution of welding and cutting. *Welding Journal*, Vol. 20, No. 5, pp. 220-34.

3. Friedman, E. (1975). Thermomechanical analysis of the welding process using the finite element method. *Journal of Pressure Vessel Technology*, Vol. 97, No. 3, pp. 206-13.
4. Goldak, J., Chakravarti, A. & Bibby, M. (1984). A new finite element model for welding heat sources. *Metallurgical Transactions B*, Vol. 15B, pp. 299-305.
5. Michaleris, P. & Debiccari, A. (1997). Prediction of welding distortion. *Welding Journal*, Vol. 76, No. 4, pp. 172-80.
6. Tsai, C. L., Park, S. C. & Cheng, W. T. (1999). Welding distortion of a thin-plate panel structure. *Welding Journal*, Vol. 78, pp. 156-65.
7. Kim, Y. C., Yamakita, T., Bang, H. S. & Ueda, U. (1988). Mechanical characteristics of repair welds in a thick plate. *International Journal of Pressure Vessels and Piping*, Vol. 32, No. 4, pp. 3-105.
8. Dong, Y., Hong, J., Tsai, C. & Dong, P. (1997). Finite element modeling of residual stresses in austenitic stainless steel pipe girth welds. *Welding J*., Vol. 76, No. 10, pp. 442-9.
9. Dong, P., Zhang, J. & Bouchard, P. J. (2002). Effects of repair weld length on residual stress distribution. *Journal of Pressure Vessel Technology*, Vol. 124, No. 1, pp. 74–80.
10. Bouchard, P. J., George, D., Santisteban, J. R., Bruno, G., Dutta, M., Edwards, L., Kingston, E. & Smith, D. J. (2005). Measurement of the residual stresses in a stainless steel pipe girth weld containing long and short repairs. *International Journal of Pressure Vessels and Piping*, Vol. 82, No. 4, pp. 299–310.
11. George, D. & Smith, D. J. (2005). Through thickness measurement of residual stresses in a stainless steel cylinder containing shallow and deep weld repairs. *International Journal of Pressure Vessels and Piping*, Vol. 82, No. 4, pp. 279-87.
12. Brown, T. B., Dauda, T. A., Truman, C. E., Smith, D. J., Memhard, D. & Pfeiffer, W. (2006). Predictions and measurement of residual stress in repair welds in plates. *International Journal of Pressure Vessels and Piping*, Vol. 83, No. 11-12, pp. 809-18.
13. Mirzaee-Sisan, A., Fookes, A. J., Truman, C. E., Smith, D. J., Brown, T. B. & Dauda, T. A. Residual stress measurement in a repair welded header in the as-welded condition and after advanced post weld treatment. *International Journal of Pressure Vessels and Piping*, Vol. 84, No. 5, pp. 265-73.
14. Aloraier, A., Al-Mazrouee, A., Price, J. W. H. & Shehata, T. (2010). Weld repair practices without post weld heat treatment for ferritic alloys and their consequences on residual stresses: A review. *International Journal of Pressure Vessels and Piping*, Vol. 87, No. 4, pp. 127-33.
15. Jiang, W., Liu, Z., Gong, J. M. & Tu, S. T. (2010). Numerical simulation to study the effect of repair width on residual stresses of a stainless steel clad plate. *International Journal of Pressure Vessels and Piping*, Vol. 87, No. 8, pp. 457-63.
16. Jiang, W. C., Wang, B. Y., Gong, J. M. & Tu, S. T. (2011). Finite element analysis of the effect of welding heat input and layer number on residual stress in repair welds for a stainless steel clad plate. *Materials and Design*, Vol. 32, No. 5, pp. 2851-57.
17. Jiang, W., Xu, X. P., Gong, J. M. & Tu, S. T. (2012). Influence of repair length on residual stress in the repair weld of a clad plate. *Nuclear Engineering and Design*, Vol. 246, pp. 211-19.
18. Roshani, M., Reihanian, M., Gheisari, K. H. & Saffarian, M. R. (2014). Evaluation of sensitization in gas tungsten arc welded AISI 304 stainless steel. *Iranian Journal of Science & Technology, Transactions of Mechanical Engineering*, Vol. 38, No. M1^{+}, pp. 207-15.
19. Fadaei, A. & Jokar, M. H. (2014). Experimental study on mechanical properties and microstructures in A 36 repair butt weldment. *Iranian Journal of Science & Technology, Transactions of Mechanical Engineering*, Vol. 38, No. M2, pp. 431-38.
20. Deng, D., Murakawa, H. & Liang, W. (2007). Numerical simulation of welding distortion in large structures. *Computer Methods in Applied Mechanics and Engineering*, Vol. 196, pp. 4613-27.

21. Barsoum, Z. & Barsoum, I. (2009). Residual stress effects on fatigue life of welded structures using LEFM. *Engineering Failure Analysis*, Vol. 16, pp. 449-67.
22. Deng, D. & Murakawa, H. (2006). Prediction of welding residual stress in multi-pass butt-welded modified 9Cr 1Mo steel pipe considering phase transformation Effects. *Computational Material Science*, Vol. 37, No. 3, pp. 209-19.
23. Goldak, J. & Akhlaghi, M. (2005). *Computational welding mechanics*. New York: Springer.